UC Berkeley
Archaeological X-ray Fluorescence Reports

Title
ENERGY-DISPERSIVE X-RAY FLUORESCENCE (EDXRF) ANALYSIS OF MAJOR, MINOR OXIDE AND TRACE ELEMENT CONCENTRATIONS FOR OBSIDIAN ARTIFACTS FROM THE MIDDLE AWASH RIVER BASIN, CENTRAL ETHIOPIA

Permalink
https://escholarship.org/uc/item/9s230639

Author
Shackley, M. Steven

Publication Date
2019-12-08

eScholarship.org Powered by the California Digital Library
University of California

GEOARCHAEOLOGICAL XRF LAB
A GREEN SOLAR FACILITY

GEOARCHAEOLOGICAL X-RAY FLUORESCENCE SPECTROMETRY LABORATORY
8100 WYOMING BLVD., SUITE M4-158 ALBUQUERQUE, NM 87113 USA

ENERGY-DISPERSIVE X-RAY FLUORESCENCE (EDXRF) ANALYSIS OF MAJOR, MINOR OXIDE AND TRACE ELEMENT CONCENTRATIONS FOR OBSIDIAN ARTIFACTS FROM THE MIDDLE AWASH RIVER BASIN, CENTRAL ETHIOPIA

DRAFT

by

M. Steven Shackley Ph.D., Director
Geoarchaeological XRF Laboratory
Albuquerque, New Mexico

Report Prepared for

Dr. Yonatan Sahle
University of Tübingen
Tübingen, Germany

8 December 2019

INTRODUCTION

The non-destructive whole rock analysis here of 17 obsidian artifacts from archaeological contexts along the Middle Awash River Basin, Ethiopia indicates a very diverse obsidian provenance assemblage similar to the diversity seen in the Negash et al. (2011) study including known and, as yet, unlocated sources. Many of those artifacts were analyzed at the Berkeley Archaeological XRF Laboratory using similar methods and calibrations (see Shackley 2005, 2019:Supplement). The results here were compared to the Negash et al. (2011) study as well as source standard data at this laboratory.

LABORATORY SAMPLING, ANALYSIS AND INSTRUMENTATION

All archaeological samples are analyzed whole. The results presented here are quantitative in that they are derived from "filtered" intensity values ratioed to the appropriate x-ray continuum regions through a least squares fitting formula rather than plotting the proportions of the net intensities in a ternary system (McCarthy and Schamber 1981; Schamber 1977). Or more essentially, these data through the analysis of international rock standards, allow for inter-instrument comparison with a predictable degree of certainty (Hampel 1984; Shackley 2011). Using non-destructive EDXRF the trace elements in the mid-Z region have been found to be the best inter-source discriminators in most regions, including the Rift Valley (Brown and Nash 2014; Shackley 2005, 2019).

The issue of accuracy using fundamental parameter calibrations of obsidian with EDXRF for whole rock non-destructive analyses has been discussed elsewhere (http://swxrflab.net/anlysis.htm). Variability can be as great as one to two percent, too great for source discrimination using non-destructive fundamental parameter analysis with EDXRF, and not necessarily as accurate as the electron microprobe results reported in Negash et al. (2011; see also Brown and Nash 2014). Further, the narrow range of variability inherent in major

oxides in rhyolites is rarely great enough for discrimination (see Glascock 2011; Glascock et al. 1998). Both Brown and Nash (2014) and these studies have shown that in East African glasses using EDXRF, the trace elements Y, Zr, Nb, Ba, at times Zn, and less so the minor elements Ti, and Mn the latter two not incompatibles, can be good source discriminators, and measured well by XRF, although Ti is not as effective in EDXRF with Si/Li detectors (Shackley 2005, 2011).

Trace Element Analyses

All analyses for this study were conducted on a ThermoScientific *Quant'X* EDXRF spectrometer, located in the Geoarchaeological XRF Laboratory, Albuquerque, New Mexico, USA equipped with a thermoelectrically Peltier cooled solid-state Si(Li) X-ray detector, with a 50 kV, 50 W, ultra-high-flux end window bremsstrahlung, Rh target X-ray tube and a 76 µm (3 mil) beryllium (Be) window (air cooled), that runs on a power supply operating 4-50 kV/0.02-1.0 mA at 0.02 increments. The spectrometer is equipped with a 200 l min^{-1} Edwards vacuum pump, allowing for the analysis of lower-atomic-weight elements between sodium (Na) and titanium (Ti). Data acquisition is accomplished with a pulse processor and an analogue-to-digital converter. Elemental composition is identified with digital filter background removal, least squares empirical peak deconvolution, gross peak intensities and net peak intensities above background.

For the analysis of mid-Z condition elements Ti-Nb ($K\alpha_1$ lines), Ce ($L\alpha_1$ lines), the x-ray tube is operated at 30 kV, using a 0.05 mm (medium) Pd primary beam filter in an air path at 100 seconds livetime to generate x-ray intensity $K\alpha_1$-line data for elements titanium (Ti), manganese (Mn), iron (as $Fe_2O_3^T$), cobalt (Co), nickel (Ni), copper, (Cu), zinc, (Zn), gallium (Ga), rubidium (Rb), strontium (Sr), yttrium (Y), zirconium (Zr), niobium (Nb), and $L\alpha_1$-line data for lead (Pb) cerium (Ce), and thorium (Th). Not all these elements are reported since their

values in many volcanic rocks are very low and often outside the detection limits. Trace element intensities were converted to concentration estimates employing a linear or quadratic calibration line ratioed to the Compton scatter established for each element from the analysis of international rock standards certified by the National Institute of Standards and Technology (NIST), the US. Geological Survey (USGS), Canadian Centre for Mineral and Energy Technology, and the Centre de Recherches Pétrographiques et Géochimiques in France (Govindaraju 1994). Line fitting is linear (XML) for all elements. When barium (Ba) and cerium (Ce) is analyzed in the High Zb condition, the Rh tube is operated at 50 kV and up to 1.0 mA, ratioed to the bremsstrahlung region (see Davis 2011; Shackley 2011). Further details concerning the petrological choice of these elements in Southwest obsidians and other volcanic rocks is available in Shackley (1988, 1995, 2005, 2011, 2019; also Mahood and Stimac 1991; and Hughes and Smith 1993). Twenty specific pressed powder standards are used for the best fit regression calibration for elements Ti-Nb, Pb, Th, Ba, and Ce include G-2 (basalt), AGV-2 (andesite), GSP-2 (granodiorite), SY-2 (syenite), BHVO-2 (hawaiite), STM-1 (syenite), QLO-1 (quartz latite), RGM-1 (obsidian), W-2 (diabase), BIR-1 (basalt), BCR-2 (basalt), SDC-1 (mica schist), TLM-1 (tonalite), SCO-1 (shale), NOD-A-1 and NOD-P-1 (oceanic manganese) all US Geological Survey standards, NIST-278 (obsidian), U.S. National Institute of Standards and Technology, BE-N (basalt) from the Centre de Recherches Pétrographiques et Géochimiques in France, and JR-1 and JR-2 (obsidian) from the Geological Survey of Japan (Govindaraju 1994).

Major and Minor Oxide Analysis

Analysis of the major oxides of Na, Mg, Al, Si, Cl (as trace element in ppm), K, Ca, Ti, Mn, and Fe, is performed under the multiple conditions elucidated below. The fundamental parameter analysis (theoretical with standards), while not as accurate as destructive analyses

(pressed powder and fusion disks) is usually within a few percent of actual, based on the analysis of the USGS RGM-1 obsidian standard (see also Shackley 2011; Table 1 here). The fundamental parameters (theoretical) method is run under conditions commensurate with the elements of interest and calibrated with ten USGS standards (RGM-1, rhyolite; AGV-2, andesite; BHVO-1, hawaiite; BIR-1, basalt; G-2, granite; GSP-2, granodiorite; BCR-2, basalt; W-2, diabase; QLO-1, quartz latite; STM-1, syenite), and one Japanese Geological Survey rhyolite standard (JR-1). The oxides are normalized to the RGM-1 USGS recommended versus measured values.

Conditions of Fundamental Parameter Analysis[1]

Low Za (Na, Mg, Al, Si, P)

Voltage	6 kV	Current	Auto[2]
Livetime	100 seconds	Counts Limit	0
Filter	No Filter	Atmosphere	Vacuum
Maximum Energy	10 keV	Count Rate	Low

Mid Zb (K, Ca, Ti, V, Cr, Mn, Fe)

Voltage	32 kV	Current	Auto
Livetime	100 seconds	Counts Limit	0
Filter	Pd (0.06 mm)	Atmosphere	Vacuum
Maximum Energy	40 keV	Count Rate	Medium

High Zb (Sn, Sb, Ba, Ag, Cd)

Voltage	50 kV	Current	Auto
Livetime	100 seconds	Counts Limit	0
Filter	Cu (0.559 mm)	Atmosphere	Vacuum
Maximum Energy	40 keV	Count Rate	High

Low Zb (S, Cl, K, Ca)

Voltage	8 kV	Current	Auto
Livetime	100 seconds	Counts Limit	0
Filter	Cellulose (0.06 mm)	Atmosphere	Vacuum
Maximum Energy	10 keV	Count Rate	Low

[1] Multiple conditions designed to ameliorate peak overlap identified with digital filter background removal, least squares empirical peak deconvolution, gross peak intensities and net peak intensities above background.

[2] Current is set automatically based on the mass absorption coefficient.

The data from the WinTrace™ software were translated directly into Excel for Windows software for manipulation and on into IGPET ver. 2000 for Windows and JMP ver. 12.0.1 for statistical analyses. In order to evaluate these quantitative determinations, machine data were compared to measurements of known standards during each run. RGM-1 a USGS obsidian standard is analyzed during each sample run of ≤19 for obsidian artifacts to check machine calibration (Table 1).

DISCUSSION

Research Trajectory

The results here were compared to results from the Negash and Shackley (2006) and Negash et al. (2006, 2011) studies and Shackley and Sahle (2017) all from sites in the Middle Awash. In the Negash and Shackley (2006) and Negash et al. (2006) studies, the trace element analysis was performed on the Spectrace/ThermoNoran *QuanX* EDXRF at UC, Berkeley the precursor to the digital *Quant'X* in Albuquerque. Shackley devised the methods and calibrated both instruments using the same international standards and the same software although the *QuanX* used an earlier version of WinTrace™ software. The results should be completely compatible with the use of the same USGS RGM-1 standard (Tables 1 and 2 and Figures 1 and

2). The oxides were analyzed by electron microprobe in the Negash et al. (2011) study, and this non-destructive fundamental parameter (theoretical) analysis here on the *Quant'X* should be relatively close, but not quite as accurate (see Brown and Nash 2014).

There has been ample work on the geology and geochronology of the region, and the dating sequence is one of the best anywhere (Brown et al. 2009; Brown and Nash 2014; Laury and Albritton 1975; Morgan et al. 2009; Negash et al. 2010, 2011; Wendorf et al. 1975, 1994; WoldeGabriel et al. 1990). Table 1 and Figures 1 and 2 here).

Major Oxides, Trace Elements, Patination and Source Assignment

Unlike many Great Rift rhyolites which are often peralkaline using the Shand Classification (1943), the oxide analysis and TAS plot indicate relatively high Si rhyolites, tightly clustered that are uniformly peraluminous ($Na_2O+K_2O<Al_2O_3$) (Table 1 and Figure 1). A conundrum in this assemblage is that sample A2B-E3-10 with a trace element concentration statistically identical to Adokoma (also written Adukoma) obsidian is significantly different in oxide concentrations and would be classified peralkaline ($Na_2O+K_2O/Al_2O_3>1$; Table 1 and Figure 1 here; see also Brown and Nash 2014; Cann 1983).

Patination in Volcanic Rocks. While there has been little research in archaeology on the effects of weathering and patination of volcanic rocks including obsidian, there has been some relevant here for geochronological studies (see Brown et al. 2009; Cerling et al. 1985; Morgan et al. 2009; Shackley and Dillian 2002). It does appear that low temperature alteration of obsidian with the inclusion of water affects Na and K concentrations, particularly an issue in dating. This process actually may be at work in this assemblage where at least the one sample (A2B-E3-10) mentioned above, a piece of patinated obsidian debitage, exhibits much higher Na and K proportions while seemingly not affecting the trace elements (see Table 1 and Figures 1

and 2). Sahle removed patination from the remainder of artifacts for this study. Shackley and Dillian found in peraluminous and peralkaline obsidian that heating near melting point (≥1000ºC) trace element concentrations are not affected (2002). The same seems to be apparent with patination although patination occurs at low temperatures (Cerling et al. 1985). Patination effects, particularly on very old volcanic glass artifacts should be examined in future obsidian studies. It does seem apparent that trace element concentrations, generally better for source assignment than the more variable lighter elements, are not significantly affected by patination or heat.

Finally, the dominance of artifacts produced from Adokoma obsidian makes sense, but as has been discussed elsewhere the number of, as yet, unlocated sources in the Great Rift Valley region hinders construction of exchange, group interaction, and social network models in archaeology (Shackley and Sahle 2009; Negash et al. 2011). The work ongoing in Ethiopia is a step in that direction, and like other regions of the obsidian world will eventually remedy this shortcoming.

REFERENCES CITED

Brown, F.H., and B.P. Nash, 2014, Correlation: Volcanic ash, obsidian. In H. Holland and K. Turekian (Eds.), *Treatise on Geochemistry*. Elsevier, Amsterdam

Cann, J.R., 1983, Petrology of obsidian artefacts. In D.R.C. Kempe and A.P. Harvey (Eds.) *The Petrology of Archaeological Artefacts*, pp. 227-255. Clarendon Press, Oxford.

Cerling, T.E., F.H. Brown, and J.R. Bowman, 1985, Low-temperature alteration of volcanic glass: hydration, Na, K, ^{18}O and Ar mobility. *Chemical Geology* 52:281-293.

Davis, K.D., T.L. Jackson, M.S. Shackley, T. Teague, and J.H. Hampel, 2011, Factors affecting the energy-dispersive x-ray fluorescence (EDXRF) analysis of archaeological obsidian. In M.S. Shackley (Ed.) *X-Ray Fluorescence Spectrometry (XRF) in Geoarchaeology*, pp. 45-64. Springer, New York.

Glascock, M.D. 2011, Comparison and contrast between XRF and NAA: used for characterization of obsidian sources in central Mexico. In M.S. Shackley (Ed.), *X-Ray*

Fluorescence Spectrometry (XRF) in Geoarchaeology, pp. 161-192. New York: Springer.

Glascock, M.D., G.E. Braswell, and R.H. Cobean, 1998, A systematic approach to obsidian source characterization. In Shackley, M.S. (Ed.) *Archaeological Obsidian Studies: Method and Theory*, pp. 15-66. Advances in Archaeological and Museum Science 3, New York: Plenum Press (now Springer).

Govindaraju, K.,1994, 1994 Compilation of Working Values and Sample Description for 383 Geostandards. *Geostandards Newsletter* 18 (special issue).

Hampel, Joachim H., 1984, Technical considerations in x-ray fluorescence analysis of obsidian. In R.E. Hughes (Ed.) *Obsidian Studies in the Great Basin*, pp. 21-25. Contributions of the University of California Archaeological Research Facility 45. Berkeley.

Hildreth, W.
1981 Gradients in Silicic Magma Chambers: Implications for Lithospheric Magmatism. *Journal of Geophysical Research* 86:10153-10192.

Hughes, Richard E., and Robert L. Smith
1993 Archaeology, Geology, and Geochemistry in Obsidian Provenance Studies. *In Scale on Archaeological and Geoscientific Perspectives*, edited by J.K. Stein and A.R. Linse, pp. 79-91. Geological Society of America Special Paper 283.

Laury, R.L., and C.C. Albritton, Jr., 1975, Geology of the Middle Stone Age archaeological sites in the Main Ethiopian Rift Valley. *Geological Society of America Bulletin* 86:999-1011.

Le Maitre, R., Bateman, P., Dudek, A., Keller, J., Lameyre, J., Le Bas, M., Sabine, P., Schmid, R., Sorensen, H., Streckeisen, A., Woolley, A., Zanettin, B. 1989, A classification of igneous rocks and glossary of terms: Recommendations of the International Union of Geological Sciences Subcommission on the Systematics of igneous rocks, Le Maitre, R.W. (Ed.). Oxford: Blackwell.

Mahood, Gail A., and James A. Stimac
1990 Trace-Element Partitioning in Pantellerites and Trachytes. *Geochemica et Cosmochimica Acta* 54:2257- 2276.

McCarthy, J.J., and F.H. Schamber
1981 Least-Squares Fit with Digital Filter: A Status Report. In *Energy Dispersive X-ray Spectrometry*, edited by K.F.J. Heinrich, D.E. Newbury, R.L. Myklebust, and C.E. Fiori, pp. 273-296. National Bureau of Standards Special Publication 604, Washington, D.C.

Morgan, L.E., P.R. Renne, R.E. Taylor, and G. WoldeGabriel, 2009, Archaeological age constraints from extrusion ages of obsidian: examples from the Middle Awash, Ethiopia. *Quaternary Geochronology* 4:193-203.

Negash, A. and M.S. Shackley, 2006, Geochemical provenance of obsidian artifacts from the Middle Stone Age site of Porc Epic, Ethiopia. *Archaeometry* 48:1-12.

Negash, A. M.S. Shackley, and M. Alene, 2006, Source provenance of obsidian artifacts from the Early Stone Age (ESA) site of Melka Konture, Ethiopia. *Journal of Archaeological Science,* 33:1647-1650.

Negash, A., F.H. Brown, M. Alene, and B. Nash, 2010, Provenance of Middle Stone Age obsidian artefacts from the central sector of the main Ethiopian Rift Valley. *Ethiopian Journal of Science* 33:21-30.

Negash, A., F.H. Brown, and B. Nash, 2011, Varieties and sources of artefactual obsidian in the Middle Stone Age of the Middle Awash, Ethiopia. *Archaeometry* 53:661-673.

Schamber, F.H., 1977, A modification of the linear least-squares fitting method which provides continuum suppression. In T.G. Dzubay (Ed.) *X-ray Fluorescence Analysis of Environmental Samples*, pp. 241-257. Ann Arbor Science Publishers.

Shackley, M. S., 1988, Sources of archaeological obsidian in the Southwest: an archaeological, petrological, and geochemical study. *American Antiquity* 53(4):752-772.

Shackley, M.S., 1995, Sources of archaeological obsidian in the greater American Southwest: an update and quantitative analysis. *American Antiquity* 60(3):531-551.

Shackley, M.S., 2005, *Obsidian: Geology and Archaeology in the North American Southwest*. University of Arizona Press, Tucson.

Shackley, M.S. 2011, An introduction to x-ray fluorescence (XRF) analysis in archaeology. In M.S. Shackley (Ed.), *X-Ray Fluorescence Spectrometry (XRF) in Geoarchaeology*, pp. 7-44. Springer, New York.

Shackley, M.S. 2019, Natural and cultural history of the Obsidian Butte source, Imperial County, California. *California Archaeology* 11:21-44, and supplement.

Shackley, M.S. and C. Dillian, 2002, Thermal and environmental effects on obsidian geochemistry: experimental and archaeological evidence. In *The Effects of Fire and Heat on Obsidian*, J.M Loyd, T. M. Origer, and D.A. Fredrickson (Eds.), pp. 117-134. Cultural Resources Publication, Anthropology-Fire History, U.S. Bureau of Land Management, Sacramento.

Shackley, M.S., and Y. Sahle, 2017, Geochemical characterization of four Quaternary obsidian sources and provenance of obsidian artifacts from the Middle Stone Age site of Gademotta, main Ethiopian rift. *Geoarchaeology* 32:302-310.

Shand, S.J. 1943, *Eruptive Rocks; Their Genesis, Composition, Classification, and Their Relation to Ore Deposits, with a Chapter on Meteorites (Revised Second Edition*). New York: Hafner Publishing Co.

Wendorf, F., R.L. Laury, C.C. Albritton, R. Schild, C.V. Haynes, P.E. Damon, M. Shafiqullah, and R. Scarborough, 1975, Dates for the Middle Stone Age or East Africa. *Science* 187:740-742.

Wendorf, F., A.E. Close, R. Shild, 1994, Africa in the period of *Homo sapiens neanderthalensis* and contemporaries. In S.J. De Laet, A.H. Dani, J.L. Lorenzo, and R.B. Nunoo (Eds.), *History of Humanity. Prehistory and the Beginnings of Civilization*, vol. 1. Routledge/UNESCO, New York, pp. 117-131.

WoldeGabriel, G., J.L. Aronson, and R.C. Walter, 1990, Geology, geochronology, and rift basin development in the central sector of the Main Ethiopian Rift. *Geological Society of America Bulletin* 102:439-458.

Table 1. Major, minor and trace element concentrations for the archaeological samples, and the USGS RGM-1 obsidian standard. Measurements in weight percent or parts per million (ppm) as noted.

Sample HAL-	Na2O	MgO	Al2O3	SiO2	K2O	CaO	TiO2	V2O5	MnO	Fe2O3	Σ
	%	%	%	%	%	%	%	%	%	%	
A2-58	3.94	1.28	14.13	67.85	5.12	1.71	0.48	0.03	0.14	4.65	99.32
A2-91	3.95	0.50	14.04	69.28	5.15	1.54	0.36	0.001	0.12	4.49	99.42
A2-355	3.78	0.29	11.93	73.09	5.38	1.08	0.37	0	0.11	3.43	99.46
A2-605	3.64	0.80	13.68	71.54	5.13	1.32	0.34	0.007	0.09	2.99	99.54
A2-606	3.26	0.58	12.32	72.68	5.30	1.46	0.39	0.009	0.09	3.38	99.45
A2-608	3.22	1.12	12.59	71.40	5.52	1.35	0.45	0.016	0.09	3.62	99.37
A2-612	2.81	2.17	13.41	70.94	5.14	1.32	0.36	0.022	0.08	3.28	99.54
A2-647	3.54	0.40	12.03	72.84	5.33	1.26	0.48	0.005	0.09	3.60	99.56
A2-669	4.50	0.49	11.32	69.89	4.44	1.09	0.54	0.015	0.16	6.61	99.05
A2-671	2.94	1.91	12.63	71.87	5.26	1.44	0.31	0	0.05	3.04	99.44
A2B-E2-163	3.89	0	11.97	75.22	5.32	0.77	0.16	0.02	0.05	2.37	99.77
A2B-E3-10	2.99	0	6.77	67.97	10.83	2.61	0.44	0.05	0.12	7.17	98.95
A2B-E3-25	4.57	0	14.86	62.47	3.34	4.56	0.93	0.03	0.16	8.27	99.18
A2B-E3-3	4.26	0	11.45	74.91	5.27	0.89	0.25	0	0.06	2.53	99.62
A2B-E3-51	4.07	0	11.50	74.52	5.48	0.88	0.23	0.001	0.07	2.88	99.62
A25B-E1-292	4.27	0	11.40	72.87	5.45	1.32	0.23	0	0.08	3.91	99.53
A25B-E1-367	4.77	0	13.45	69.66	5.21	1.51	0.33	0	0.11	4.11	99.17
RGM1-S4	3.85	0	12.86	74.03	5.02	1.39	0.27	0.013	0.04	2.27	99.74
RGM-1 recommended	4.07	0.28	13.70	73.40	4.30	1.15	0.27	nr	0.04	1.86	

Sample HAL-	Cl	Zn	Rb	Sr	Y	Zr	Nb	Ba	Ce	Source
	ppm	ppm	ppm	ppm	ppm	ppm	ppm	ppm	ppm	
A2-58	3777	95	133	65	58	507	73	861	125	10
A2-91	2844	109	136	59	54	519	77	887	162	10
A2-355	2396	98	155	35	78	374	48	1031	133	Adokoma
A2-605	2388	75	118	64	53	299	47	746	138	12
A2-606	2445	95	160	37	81	390	53	1021	141	Adokoma
A2-608	3368	102	170	36	89	404	43	1016	132	Adokoma
A2-612	2256	108	168	38	81	391	44	966	136	Adokoma
A2-647	1560	105	171	40	85	399	53	997	156	Adokoma
A2-669	6037	299	94	27	105	777	160	880	181	11

Sample HAL-	Cl	Zn	Rb	Sr	Y	Zr	Nb	Ba	Ce	Source
A2-671	3047	108	170	38	85	391	49	951	141	Adokoma
A2B-E3-3	598	118	168	40	87	383	48	856	83	Adokoma
A2B-E3-10	4096	126	171	33	83	389	46	1023	96	Adokoma?
A2B-E3-25	3794	146	79	195	81	751	56	1611	155	unknown
A2B-E3-51	2148	118	183	39	89	408	57	1002	88	Adokoma
A2B-E2-163	1537	129	162	45	86	414	58	988	133	Adokoma
A25B-E1-292	1689	109	163	71	90	394	51	1024	118	Adokoma
A25B-E1-367	5559	104	145	64	62	552	91	1016	116	10
RGM1-S4	655	40	143	113	24	223	9	788	49	standard
RGM-1 recommended	510	32	150	110	25	220	9	810	47	

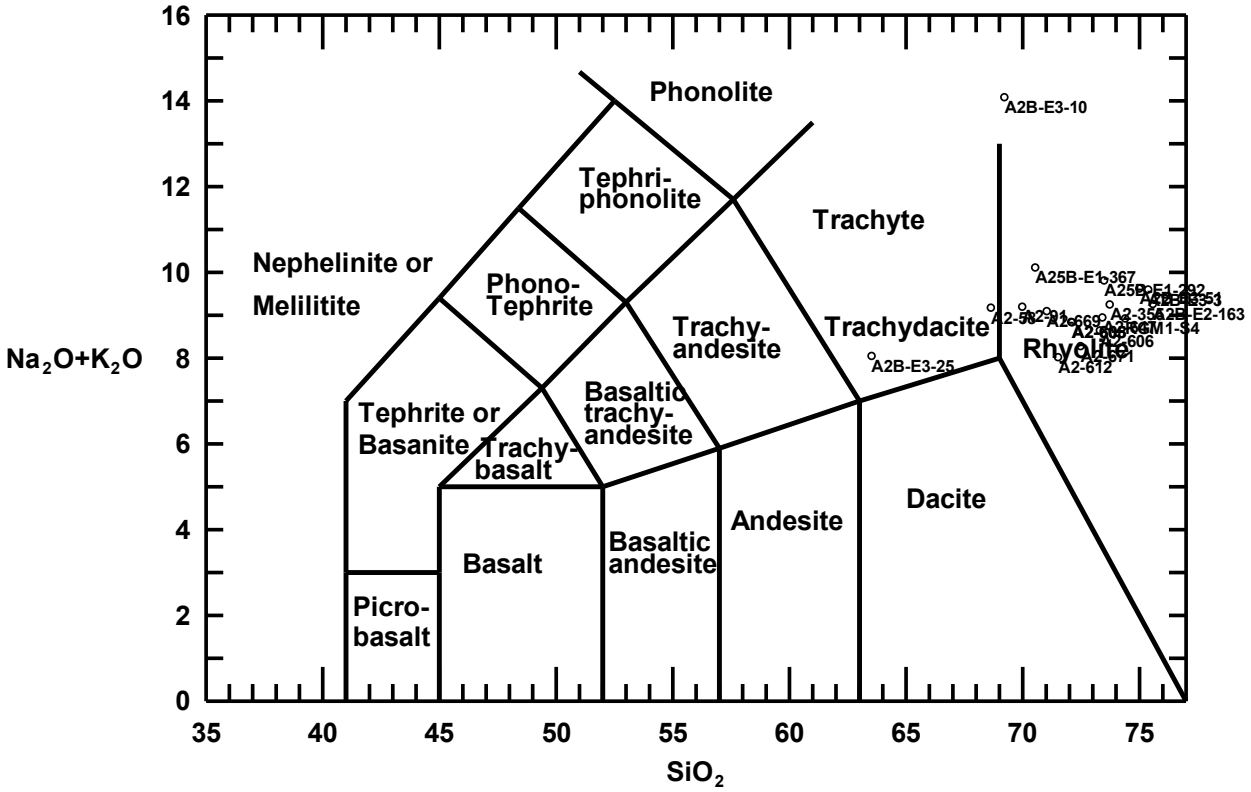

Figure 1. TAS plot of a the archaeological samples and USGS RGM-1 rhyolite standard (Le Maitre et al. 1989).

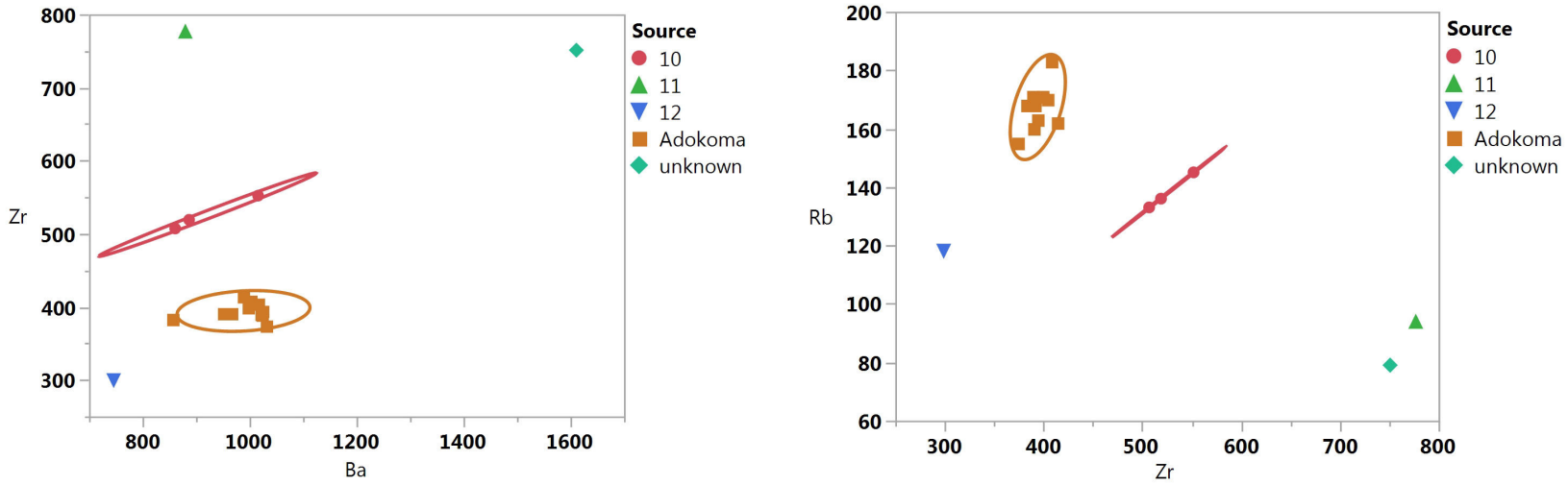

Figure 2. Ba/Zr and Zr/Rb bivariate plots of the archaeological samples. Confidence ellipses at 95%.